

# Kent Academic Repository

## Full text document (pdf)

### Citation for published version

Miller, Christopher N. and Panagos, Charalampos G. and Mosedale, William R. T. and Kvac, Martin and Howard, Mark J. and Tsatsou, Anastasios D (2017) Effects of Cryptosporidium infections on host cell metabolome and host mitochondrial associations. *mSphere*. (Submitted)

### DOI

<https://doi.org/10.1101/145979>

### Link to record in KAR

<http://kar.kent.ac.uk/64570/>

### Document Version

Pre-print

#### Copyright & reuse

Content in the Kent Academic Repository is made available for research purposes. Unless otherwise stated all content is protected by copyright and in the absence of an open licence (eg Creative Commons), permissions for further reuse of content should be sought from the publisher, author or other copyright holder.

#### Versions of research

The version in the Kent Academic Repository may differ from the final published version.

Users are advised to check <http://kar.kent.ac.uk> for the status of the paper. **Users should always cite the published version of record.**

#### Enquiries

For any further enquiries regarding the licence status of this document, please contact:

[researchsupport@kent.ac.uk](mailto:researchsupport@kent.ac.uk)

If you believe this document infringes copyright then please contact the KAR admin team with the take-down information provided at <http://kar.kent.ac.uk/contact.html>

1   **Effects of *Cryptosporidium* infections on host cell metabolome and**  
2   **host mitochondrial associations**

3

4   Running Title: ***Cryptosporidium*-host metabolomic interactions**

5

6   **Christopher N. Miller<sup>1</sup>, Charalampos G. Panagos<sup>2,6</sup>, William R. T. Mosedale<sup>1</sup>,**  
7   **Martin Kváč<sup>3,4</sup>, Mark J. Howard<sup>2,5</sup> & Anastasios D. Tsaousis<sup>1\*</sup>**

8

9   <sup>1</sup>Laboratory of Molecular & Evolutionary Parasitology, RAPID group, School of  
10 Biosciences, University of Kent, Canterbury, UK

11   <sup>2</sup>Biomolecular NMR facility, School of Biosciences, University of Kent, Canterbury, UK

12   <sup>3</sup>Institute of Parasitology, Biology Centre CAS, České Budějovice, Czech Republic

13   <sup>4</sup>Faculty of Agriculture, University of South Bohemia in České Budějovice, České  
14 Budějovice, Czech Republic

15   <sup>5</sup>Centre for Microscopy, Characterisation and Analysis & School of Molecular Sciences,  
16 The University of Western Australia, Bayliss Building M313, Perth WA 6009, Australia.

17   <sup>6</sup>Current address: Complex Carbohydrate Research Center, University of Georgia,  
18 Athens, GA, 30602, USA

19   **\* Correspondence:**

20   Dr. Anastasios D. Tsaousis

21   [A.Tsaousis@kent.ac.uk](mailto:A.Tsaousis@kent.ac.uk)

22

23

24     **Abstract**

25     *Cryptosporidium* is an important gut microbe whose contributions towards infant and  
26     immunocompromise patient mortality rates are steadily increasing. However, current  
27     techniques for studying the parasite are few and far between, relying on a combination  
28     of *in-silico* predictions and medical reports. The development of an *in-vitro* culture  
29     system, using COLO-680N cells (derived from an esophageal squamous cell  
30     carcinoma), has provided the *Cryptosporidium* community with the opportunity to  
31     expand its toolkit for investigating this disease. One area in particular that is sorely  
32     overlooked is the effect infection has on host metabolic processes, especially those of  
33     the host mitochondria, which have been shown anecdotally in previous studies as being  
34     in abundance surrounding the sites of infection. Using a  $^1\text{H}$  Nuclear Magnetic  
35     Resonance approach to metabolomics, we have explored the nature of the mouse gut  
36     metabolome as well as providing the first insight into the metabolome of an infected cell  
37     line. Through a combination of Partial Least Squares Discriminant Analysis and  
38     predictive modelling, we demonstrate new understandings of the effects of a  
39     *Cryptosporidium* infection, while verifying the presence of known metabolic changes. Of  
40     particular note is the potential contribution of host derived taurine to the diuretic aspects  
41     of the disease previously attributed to a solely parasite based alteration of the gut  
42     environment. This practical and informative approach can spearhead our understanding  
43     of the *Cryptosporidium*-host metabolic exchange and thus provide novel targets for  
44     tackling this deadly parasite.

45

46

47    **Importance**

48    Cryptosporidiosis is a diarrheal disease caused by *Cryptosporidium*, a pathogen of  
49    great medical importance. Reports on the infection patterns of the parasite and its  
50    interactions with the host are very limited. Using a combination of NMR metabolomics  
51    and cell biological techniques, we have shown molecular host-parasite interactions,  
52    using both infected mice and the COLO-680N cell line that successfully propagates the  
53    parasite. Of major importance are our observations that the host mitochondria have  
54    changed their localisation, assembly and production, upon infection by the parasite. Our  
55    results also demonstrate further evidence that COLO-680N can be used as a model to  
56    investigate these interactions and host manipulation by the parasite. In summary, we  
57    present the molecular interactions between *Cryptosporidium* and its host, generate  
58    essential knowledge about this medically important pathogen, confirm further the validity  
59    of the COLO-680N model of infection and we are providing suggestions of potential new  
60    targets for anti-parasitic drug development.

61

62

63

64

65

66

67

68    **Introduction**

69    Cryptosporidiosis is a disease characterised by prolonged episodes of intense diarrhoea  
70    and is the second largest cause of diarrhoeal disease and death in infants across Africa  
71    and South Asia, the aetiological agents are apicomplexan parasites: the *Cryptosporidia*  
72    (1-4). Cryptosporidiosis is also amongst one of the common diseases of the  
73    immunocompromised, particularly HIV positive patients who are at 75-100% risk of  
74    contracting the disease during their lifetime, with the specific species of *Cryptosporidium*  
75    responsible being either *Cryptosporidium parvum* or *Cryptosporidium hominis* (3, 5-9).  
76    Infection occurs when an individual ingests the oocysts of the parasite, often swallowing  
77    a contaminated water source. Water treatment options are limited to filtering or boiling,  
78    which are generally not possible at an industrial scale and UV treatment, which is both  
79    expensive and rarely in place prior to outbreaks. Failing this, treatment is typically  
80    rehydration, although one drug has been shown to be effective, the broad spectrum  
81    anti-parasitic Nitazoxanide (10). However, the drug is far from ideal and displays a  
82    range of undesirable side effects including cytotoxicity and nausea, as well as being  
83    limited to use in cases where the patients are immunocompetent (11-14).

84    Until recently, a significant barrier to research into cryptosporidiosis has been the  
85    absence of a combined long-term *in vivo* culturing system and comprehensive model of  
86    host parasite interactions in addition to a heavy reliance on antibody based detection  
87    both in the scientific and the medical field (2, 4, 12, 15-19). Recent papers have  
88    attempted to rectify this by proposing improved or entirely novel techniques for culturing  
89    the parasite *ex-vivo* in tissue cultures, using the cultured cancer cells as host cells (18,  
90    20). A recent study identified that infections of COLO-680N cell cultures produced a

91 longer term and higher production volume culture of the parasite compared to  
92 previously existing *in-vitro* cultures (21). These advances have allowed higher in depth  
93 microscopy-based studies and even promise to provide a solution to developing a  
94 genetic engineering platform for the parasite. However, beyond microscopy and  
95 localisation studies, the knowledgebase of the host parasite interaction remains largely  
96 undeveloped (4, 13, 14, 22, 23).

97 One area lacking study is metabolomics. Only two peer-reviewed publications have  
98 explored the concept of the infection metabolome, one on mice and the other on human  
99 faecal samples, both showing a clear relation between infection and change in  
100 metabolite levels (24, 25). While working on different sample sources, each identified  
101 the hexadecanoic acid as a significant contributor to the change in the metabolome  
102 during infection. Previous studies noticed a number of metabolites, mainly amino acids,  
103 decreased in relative abundance in infected mice faeces compared to an increase seen  
104 previously in humans (24). This was explained to be most likely due to the inherent  
105 variation between the different host species metabolomes, as highlighted by Saric et al.  
106 in 2008 and highlights a pressing need for further and wider reaching studies into the  
107 metabolome of *Cryptosporidium* infections as well as the development and application  
108 of different techniques beyond the Gas Chromatography Mass Spectrometry (GC-MS)  
109 used in those papers (24-26).

110 Currently, the majority of metabolomics studies utilise a GC-MS approach, with great  
111 success, however  $^1\text{H}$  Nuclear Magnetic Resonance (NMR) metabolomics can be used  
112 as an additional or alternative powerful tool for metabolic screening.  $^1\text{H}$  NMR is a simple  
113 method that allows for a comparatively lossless analysis of metabolites, with fewer

114 steps between sample recovery and analysis than GC-MS, which offers a huge  
115 advantage for studies involving field samples (26-30). This translates to a more reliable  
116 result in terms of quantification and reproducibility. As such, NMR has already seen use  
117 in analysing the profile of *Plasmodium falciparum*, although the metabolome of the  
118 apicomplexan parasite as a whole is almost entirely unexplored (31).

119 Here we attempted to investigate the host-parasite interactions, using a combination of  
120 microscopy and  $^1\text{H}$  NMR approaches. In COLO-680N cell biological studies, we  
121 observed peculiar interactions between the intracellular, but extracytoplasmic, parasite  
122 and its host's mitochondria (21). These observations were even further explored by  
123 analysing cryptosporidiosis-induced changes, which we biochemically investigated  
124 using a  $^1\text{H}$  NMR approach. In addition, we have applied the same NMR based  
125 methodology to infected mice guts, in order to study the similarities and differences  
126 displayed between *in-vivo* and *in-vitro* models and identify potential cross-species  
127 markers of infection.

128

## 129 **Results**

### 130 *Host mitochondria during infection*

131 To investigate the cellular role of host organelles during infection, we employed an  
132 Indirect Fluorescence Assay (IFA) approach to determine whether the organelles,  
133 particularly the mitochondria, of the host cells were responding to a *Cryptosporidium*  
134 infection (**Figure 1**). Our results demonstrated that on multiple occasions,  
135 approximating 80-90% of infected cells, the host mitochondria were shown to

136 congregate in larger densities near the *Cryptosporidium* infection, with a corresponding  
137 increase in labelling intensity compared to uninfected areas, indicative of stronger  
138 mitochondrial metabolic activity (**Figures 1; Videos 1-3**). Transmission Electron  
139 Microscopy images of infected cells also showed host mitochondrial congregation  
140 around the parasitophorous vacuole (**Figure 2**). Interestingly, in infected cell cultures we  
141 observed, cytoskeletal structures (either actin or tubulin) were seen to conjugate with  
142 the host mitochondria, “pulling” them around the parasitophorous vacuole, in response  
143 to the infection by the parasite.

144

145 *Cell culture sample extractions*

146 Extrapolated NMR data from COLO-680N (n = 38, *C. parvum* Iowa = 12, Control = 12,  
147 *C. hominis* = 7, *C. parvum* Weru = 7) metabolite extractions, demonstrated clear  
148 differences between the *Cryptosporidium* used in comparison to both the control and  
149 other infections; each set of spectra within a group appeared visually identical both  
150 between each individual sample and their technical repeats, indicating reliable spectra  
151 acquisition (**Figure 3a**). Readily visible differences could be seen between creatine,  
152 creatine phosphate, taurine and lactate (**Figures 3b-d**) were readily visible in the raw  
153 spectra. Chenomx analysis produced a list of 161 total compounds of varying  
154 concentrations across samples (**Figure 4**). The PCA generated by the same statistical  
155 analysis as before, produced ample separation of the *Cryptosporidium*-infected and  
156 uninfected cultures in multiple experiments (**Figure 5a and 5c**). Furthermore, the  
157 separation of the individual infection groups suggests that differences between both  
158 *Cryptosporidium* species and within individual strains of *C. parvum*, may illicit different

159 metabolic responses in cell cultures. It is important to note that all data obtained from  
160 the 38 individual samples was input into the calculations, as there was insufficient  
161 evidence to suggest any were statistical outliers. The loading scores plot of the PCA  
162 showed a number of amino acids contributed heavily to the separations between  
163 groups, such as lactate, several fatty acid derivatives and taurine (**Figure 5b**).

164 Any and all metabolites identified in this manner were input into an online tool  
165 (MetaboAnalyst 3.0) producing a graph detailing which metabolic pathways were  
166 influenced by infection (**Figure 6a**) (32). This approach identified several pathways,  
167 including the biosynthesis of various amino acids, as well as ketones and CoA (**Figure**  
168 **6b-f**). Within these pathways, metabolites were highlighted that were identified via the  
169 PCA as contributing reliably towards differences between groups. Full compound  
170 names are available in **Supplementary Figure 1**.

171 *Mice faecal sample extractions*

172 Faecal samples from infected and uninfected mice were smeared onto microscope  
173 slides and stained with a aniline-carbol-methyl violet method, allowing the detection of  
174 *C. parvum* oocysts and thus validation of successful infections (**Supplementary Figure**  
175 **2**). Samples from both control and infected mice were taken at ten days' post infection.  
176 The spectra produced by the NMR showed clear distinctions between the infected and  
177 uninfected mice, as well as distinctions between the different strains of infections  
178 (**Figure 7a**). Though 38 individual experiments were used to produce this data, the  
179 validity and reliability of each was confirmed by performing a further 9 technical replicate  
180 NMR scans. Several metabolites were readily distinguishable prior to the metabolomics  
181 analyses, including indicators of phosphorylation; taurine (**Figure 7b**), creatine and

182 creatine phosphate (**Figure 7c**) and lactate (**Figure 7d**). Processing the data from the  
183 mice guts ( $n = 18$ , six per infection) via the Chenomx Nmr Suite version 8.2 platform  
184 produced a list of 151 compounds that were extrapolated from the spectra (**Figure 8**).  
185 Statistical analysis of the data, with freely available Microsoft Excel Add-in “multi-base  
186 2015”, by Partial Least Squares Discriminant Analysis (PLS-DA) determined notable  
187 separation of the three conditions, (uninfected control, *C. parvum* Iowa II and *C. parvum*  
188 Weru infections), whilst maintaining group cohesion (**Figure 9a**). The loading values of  
189 the variable compound contributions (**Figure 9b**), suggest certain metabolites were  
190 more significant to the separation of the groups than others. The presence of L-alanine  
191 and valine, two common amino acids, agrees with the previous literature and 2-  
192 oxoisocaproate is a component of the valine/leucine/isoleucine biosynthetic pathways  
193 reports (24, 25).

194 MetaboAnalyst 3.0 based analysis of the metabolites proposed that a number of amino  
195 acid biosynthesis pathways could be altered during the course of an infection, such as  
196 the glycine, valine and taurine pathways. In addition, the mice infections displayed  
197 possible changes to other metabolic pathways (**Figure 10a**) as those pathways furthest  
198 from the x, y axis intercept, representing both the overall completeness of the pathways  
199 and number of contributing detected metabolites respectively. As with **Figures 6a-g**, the  
200 pathways identified in the manner, and the compounds discovered by the NMR  
201 demonstrated that infections caused changes in at least the valine (**Figure 10c**), glycine  
202 (**Figure 10d**) and taurine amino (**Figure 10e**) acid biosynthetic pathways, in addition to  
203 several sugar pathways (**Figure 10b, f, g**). As before, full compound names are  
204 available in **Supplementary Figure 1**.

205

206 *Comparison of mice faecal and COLO-680N metabolome changes*

207 MetaboAnalyst data from **Figure 6** and **Figure 10**, demonstrate that a number of altered  
208 pathways are shared between the mice and tissue culture metabolites, particularly  
209 taurine and amino acid metabolic pathways. Taurine is involved in a number of roles,  
210 including bile acid conjugation, osmoregulation, membrane integrity and protection  
211 against oxidative free radicals. Glycine synthesis was also shown to be affected to a  
212 large degree and is involved with numerous and diverse cellular functions including  
213 purine synthesis, basic protein construction and provides the building blocks for  
214 porphyrins (33, 34). All of these pathways have a direct or indirect impact on the host's  
215 mitochondrial energetic activity. Comparing the data from the mouse and cell culture  
216 responses directly revealed a large number of metabolite level responded similarly to  
217 infection regardless of host (**Figures 11a and b**). Interestingly, although the  
218 mitochondria remained the most likely site of metabolic change, regardless of host or  
219 parasite, the metabolites in question did change depending on the parasite strain  
220 involved.

221

## 222 **Discussion**

223 Previous studies (21) recently demonstrated the successful long-term propagation of  
224 *Cryptosporidium parvum* in COLO-680N cell culture. Their studies have shown the  
225 presence of organelles around the parasite (e.g. feeder organelle), which implied a  
226 direct association between the parasite and the host. This host-parasite relation became

227 more intriguing when we observed a close relation between the host mitochondria and  
228 the parasite during infection. To investigate this even further, we have used a  
229 combination on mitochondrial assays, which have shown higher mitochondrial activity in  
230 infected cells and  $^1\text{H}$  NMR to explore the metabolomics of the infection.

231 Solution-state  $^1\text{H}$  NMR offers a practical approach to metabolomics that is especially  
232 useful where sample volume sizes are particularly small (27, 30, 35). Although GC-MS  
233 holds an advantage for detecting low-levels of metabolites with unique mass signatures,  
234 for the purpose of determining the change in metabolite quantities, NMR provides a  
235 viable alternative (26-31). Initial analysis of our data showed a clear distinction between  
236 the metabolic fingerprints of infected and uninfected samples, even between infections  
237 of different strains of the parasite to some extent; with PCA producing distinct groups of  
238 metabolite profiles, correlating to uninfected and infected samples (**Figure 5a and c**).  
239 This may in-part be explained as the manifestation of the biochemical differences  
240 between the species which contribute to their observed species specificity

241 Of particular importance is the degree to which these results, both from the *in-vitro* and  
242 *in-vivo*, agree with the previous literature. Our study also demonstrates that metabolic  
243 compounds L-alanine, isoleucine and succinic acid (succinate) were detected as  
244 contributors to the variance between the sample conditions that indicated infection.  
245 Moreover, even though valine was not detected in the uninfected controls, it was visible  
246 in the infected samples and in agreement with previous studies (24, 25).

247 The MetaboAnalyst data revealed a number of pathways were potentially influenced by  
248 infection, including several that showed changes in both the mice and cell culture  
249 experiments, such as amino acid and CoA biosynthesis. Support for these findings is

250 observed via the biosynthesis pathways for alanine and glycine that were highlighted  
251 previously in GC-MS studies as being potentially influenced by infection (24, 25)

252 As a parasite, *Cryptosporidium* is dependent on host derived biosynthetic pathways for  
253 survival. For example, *C. parvum* is incapable of producing the majority of amino acids  
254 *de-novo*, instead relying heavily on the import of host metabolites via active channelling  
255 (36). The biosynthetic pathway for glycine, threonine and serine was upregulated, in  
256 both cell culture and animal experimentations, with particularly high levels of glycine  
257 detected. Both *C. parvum* and *C. hominis* are incapable of manufacturing these amino  
258 acids *de novo*, instead relying on scavenging host serine and glycine, utilising serine  
259 and glycine hydroxymethyltransferases to convert one to the other when needed (36,  
260 37). The reliance on host amino acids could provide a novel method for combating the  
261 infection, based upon previous studies that identified other amino acid metabolic chains  
262 as potential targets (37, 38). For example, glycine reuptake inhibitors (GRIs) that are  
263 often used in treating schizophrenia, could be utilised to partially starve the parasite of  
264 the metabolite.

265 In addition to the amino acid biosynthesis pathways, it is also apparent that taurine  
266 synthesis is also implicated in the metabolic profile of the disease as shown in the  
267 presented analyses; taurine has frequently been used in the past as an agent for  
268 inducing excystation for *in-vitro* cultures as sodium taurocholate (39-42). In the host,  
269 taurine has a number of roles, those relevant to the cell types involved include: cell  
270 membrane integrity, osmoregulation and adipose tissue regulation. Previous  
271 metabolomic studies of faecal samples from *Cryptosporidium*-infected patients revealed  
272 increased taurine concentrations, explained by the characteristic decline in gut

absorption as a result of villi malformation by the parasite (43, 44). However, an even greater increase in taurine levels was observed in the infected COLO-680N cell cultures, wherein malabsorption is not an applicable explanation. In addition to the pathways and the relevant metabolites featured in **Figures 6** and **10**, there were also a number of potentially important metabolites not represented. Increases were also observed in the abundance of adenosine derivatives (AMP, ADP and ATP); all showing an increased abundance in infected cells and mice in *C. parvum* Iowa II infections, along with a similar increase in creatine levels in *C. parvum* Weru infections. This implicates the role of host mitochondria in the context of infection as each species and strain used lacks the creatine kinase needed to produce creatine phosphate, which typically operate in localisation with mitochondria. Levels of pyruvate in *C. hominis* cell and pantothenate in *C. parvum* Iowa II infections suggest a role for oxidatative phosphorylation. This is of particular interest as the *C. parvum* genome contains a sequence for a potential pantothenate scavenging protein (45). Moreover, the further increase in lactate levels detected in *C. hominis* cell cultures and *C. parvum* Iowa II mouse infected samples, compared to the controls, indicate a strong contribution from anaerobic pathways most likely from the host. This suggests that more ATP is being produced than the oxidative capacity of the host mitochondria can maintain, producing a net increase in lactate as the oxygen debt increases. Similar observations have been made in other intracellular parasites, including the microsporidian *Encephalitozoon cuniculi*, in which the organism acquired specialized transporters to overcome its needs for ATP (46).

295 These data suggest that *C. parvum* and *C. hominis* infections may be directly or  
296 indirectly inducing an increase in host mitochondrial activity. If factual, this would result  
297 in a large number of oxygen free radicals being produced by the metabolic machinery.  
298 Consequently, cell(s) would respond with a matching increase in the synthesis of  
299 antioxidants such as taurine, which also sees increases during infection (47-49).  
300 Support for this hypothesis can be seen in the way host mitochondria appear to  
301 congregate around the *Cryptosporidium* infection (e.g. parasitophorous vacuole)  
302 (**Figures 1 and 2**). Nevertheless, taurine also plays another role within cells, for  
303 example as a diuretic. Taurine is involved in the maintenance of the ionised forms of  
304 magnesium and potassium within the cell, producing a diuretic effect that may  
305 contribute towards the characteristic water-loss of a patient with cryptosporidiosis (43,  
306 50-52). Furthermore, it has been found that taurine levels influence production of short  
307 chained fatty acid, another aspect of host biology theorised to be scavenged by *C.*  
308 *parvum* and *C. hominis* (52-54). The detection of a rise in taurine levels *in-vitro* further  
309 suggest that the increase in taurine typically detected in cryptosporidiosis patients' stool,  
310 is more than simply the result of the guts decrease in absorptive qualities. It is likely that  
311 the intra-cellular role of taurine in this disease has been overlooked and that the  
312 pathophysiology of this disease is more complicated than currently understood, and  
313 extends beyond simple villi degradation.

314 Lastly, these results alone suggest the option of determining infections via a possible  
315 comparative  $^1\text{H}$  NMR of patient and reference biopsies. This method offers an  
316 alternative approach in the medical field, where current methods of diagnosis are reliant  
317 on separate methods to achieve the same result as NMR, with infections detected by

318 laborious and often inaccurate microscopy and strain typing dependant on successful  
319 PCR.

320 In conclusion, we have demonstrated for the first time that the use of  $^1\text{H}$  NMR in the  
321 context of both medical and scientific applications is indispensable in the fight against  
322 cryptosporidiosis. With the application of a more user-friendly and reproducible  
323 approach of metabolomics, through the  $^1\text{H}$  NMR methodology described in this paper, it  
324 will now be easier for the *Cryptosporidium* community to further explore the remaining  
325 aspects of the disease metabolome in patients' samples. Future experiments could  
326 include similar investigations of other *Cryptosporidium* species and their published *in*  
327 *vitro* cell cultures or an in-depth analysis of one of the many compounds identified in this  
328 paper. Additionally, elucidating the more pathogenic influences of taurine biosynthesis  
329 in the pathobiology of cryptosporidiosis is critical. With these data, a metabolomics  
330 based method of diagnosing and treating the disease could become a reality.

331

332 **Materials and Methods**

333 *Cryptosporidium*

334 Three isolates of *C. parvum* were used in this study. The reference strain *C. parvum*  
335 Iowa II was obtained from Bunch Grass Farm in the United States, isolated from  
336 infected calves. The human isolate *C. parvum* Weru strain was supplied courtesy of Dr  
337 Martin Kváč of the Institute of Parasitology Biology Centre CAS, Czech Republic. The  
338 Weru strain was originally isolated from an infected human patient and subsequently  
339 maintained by passing through SCID mice. The final isolate used was the human isolate

340 of *C. hominis*, supplied courtesy of Prof. Rachel Chalmers from the *Cryptosporidium*  
341 Reference Unit, Singleton Hospital of NHS Wales.

342 *Tissue culture*

343 75 cm<sup>2</sup> monolayers of COLO-680N were infected and maintained as per the protocols  
344 outlined previously (21), using all three isolates of *Cryptosporidium*. A control group was  
345 also established, following the same protocols as the infections, absent oocysts. Two  
346 separate experiments were executed using a minimum of five flasks per sample  
347 condition.

348 *Animals and infection*

349 For this study, seven day old BALB/c mice were infected at the Institute of Parasitology,  
350 Biology Centre CAS using pre-established protocols detailed in Meloni and Thompson,  
351 totalling five mice per condition (55). Balb/c were chosen due to their similar response to  
352 infection as a healthy adult male. Three separate conditions, totaling six animal each,  
353 were used, infecting with 100,000 oocysts of *C. parvum* Iowa II, 100,000 oocysts of the  
354 *C. parvum* Weru isolate or a PBS control, given by oral gavage. The groups were kept  
355 physically separated and never allowed to interact. Infection was monitored from Day-1  
356 post-infection by aniline-carbol-methyl violet staining of faecal smears staining of faecal  
357 smears, in addition to an antigen based strip test (56), RIDA®QUICK *Cryptosporidium*,  
358 supplied by R-Biopharm. At ten days' post-infection, the mice were euthanized by  
359 cervical dislocation and decapitation. Samples of the ileum were dissected from the  
360 mice, measured to the same size to ensure reproducibility. This study was carried out in  
361 accordance with Act No 246/1992 Coll. of the Czech Republic. The protocol was

362 approved by the Committee for Animal Welfare of Biology Centre Czech Academy of  
363 Science and the veterinary administration authorities with regards to the animal  
364 experiments, (experiment reference numbers: 114/2013 and 52/2014).

365 *Sample preparation for NMR*

366 The following protocol was adapted from published and well-established metabolic  
367 extraction methods used for NMR-based untargeted analysis of cell extracts (57-60).  
368 Animal samples were retrieved from the contents of the ileum and surrounding intestinal  
369 structure by dissecting out the area of interest and washing through with 3 ml 100%  
370 ethanol at room temperature via syringe inserted into the opening, collecting the wash  
371 through.

372 Collected samples were then centrifuged for three minutes at 10,000 g, the supernatant  
373 discarded and the pellet weights recorded. The samples were then suspended by vortex  
374 in 2 ml of 75% ethanol, pre-heated to 80°C, to immediately inhibit subsequent metabolic  
375 reactions, then transferred to a new tube and an additional five ml of 75% ethanol  
376 added.

377 2 ml of 2 mm diameter glass beads were added to the samples and agitated by vortex  
378 for 30 seconds before incubating the samples for three minutes at 80°C. The samples  
379 were vortexed for a further 30 seconds or until the sample was completely  
380 homogenised. Tissue culture samples were collected by draining the media, adding 6  
381 ml of ethanol at 80°C to the culture flask and scraping the cells off the surface by cell  
382 scraper, transferring the mixture of lysed cells into 15 ml polyethylene tubes via a 10-ml  
383 serological pipette.

384 The samples were then transferred into 2 ml tubes, retaining the glass beads in 15 ml  
385 conical tubes. The beads were washed with an additional two ml of 80°C, 75% ethanol  
386 and again the liquid was transferred into sterile 2 ml tubes, retaining the glass beads in  
387 the tube.

388 Cell debris and general detritus were removed from the samples by centrifugation at  
389 16,000 g for 10 minutes and the resulting supernatant transferred to new, sterile 2 ml  
390 microcentrifuge tubes. The samples were then dried via Rotorvac for 12 hours or until  
391 completely desiccated, at 40°C, suspended in 330 µl double distilled water and  
392 centrifuged at 2,500 g for 10 minutes. The supernatants were recombined into ~1 ml  
393 aliquots per original sample in sterile 1.5 ml microcentrifuge tubes and frozen at -20 °C  
394 until the day before NMR analysis. The sample tubes are subsequently placed into a  
395 freeze drier until completely desiccated, suspended in 1 ml of deuterium oxide ( $^2\text{H}_2\text{O}$ )  
396 and spiked with the sodium salt of the calibration and quantitation control compound: 3-  
397 (Trimethylsilyl)-1-propanesulfonic acid (DSS), to a final concentration of 20 µM and a  
398 tested pH of 7.5.

399 *NMR protocol and analysis*

400 Samples were analysed using a 4-channel Bruker Avance III 14.1 T NMR spectrometer  
401 (600 MHz  $^1\text{H}$ ) equipped with a 5 mm QCI-F cryoprobe. For controls: six separate,  
402 uninfected 25 cm<sup>2</sup> COLO-680N 100% confluent monolayer cultures were analysed in  
403 addition to three uninfected BALB/c mice. Infected samples consisted of six 25 cm<sup>2</sup>  
404 COLO-680N 100% confluent monolayers in addition to three Iowa infected BALB/c and  
405 three Weru infected BALB/c mice. One dimension NMR datasets were acquired with a  
406 pulse repetition rate of 5 s over 128 scans, preceded by eight equilibrating dummy

407 scans and suppression of the residual Deuterium Oxide solvent (HDO) resonance using  
408 presaturation. This was repeated 5 times per sample in order to ensure the reliability of  
409 the spectra produced. Processed NMR spectrographic datasets were produced by  
410 Topspin 3.2 and analysed using Chenomx NMR Suite version 8.2. Partial Least  
411 Squares Discriminant Analysis (PCA) of the Chenomx data were generated with the  
412 freely available Microsoft Excel Add-in “multi-base 2015” by Numerical Dynamics,  
413 Japan (61) and “Past3.x” by Øyvind Hammer, Natural History Museum, University of  
414 Oslo. Pathway predictions were produced by the MetaboAnalyst 3.0 web tool, using a  
415 hypergeometric test and relative-betweenness centrality against *Homo sapiens* and *Mus*  
416 *musculus* databases for the tissue culture and mouse models respectively (32).

417 *Indirect Fluorescence Assays*

418 COLO-680N cultures were seeded onto Lab-Tek, two well, Permanox chamber slides  
419 (Sigma Aldrich, Cat No. Z734640) and allowed to reach 70% confluence before  
420 infecting, following previously published protocols (21). At seven days post infection the  
421 media was aspirated from the cultures and washed twice with 1 x PBS. Fresh, pre-  
422 warmed RPMI-1640 (Sigma Aldrich, Cat. No R8758) (1% Antibiotic/Antimycotic)  
423 containing 200 nM Thermofisher Mitotracker Red CMXRos (Molecular probes; Cat. No  
424 M7512), was added to the wells and incubated in the dark at 37°C for 45 minutes. The  
425 media was removed and replaced with further pre-warmed RPMI-1640 (1%  
426 Antibiotic/Antimycotic), containing 3.5% formaldehyde, for 15 minutes at 37°C as per  
427 the manufacturer’s protocol. The cells were then briefly permeabilised with 0.2% Triton-  
428 x100 in 1x PBS for 10 minutes, washed twice with 1x PBS and four drops of  
429 SporoGlo™ (sensitive to *Cryptosporidium* life cycle stages, excluding the oocyst) or

430 Crypt-a-glo™ (WATERBORNE, INC) (less sensitive to intracellular life cycle stages but  
431 sensitive for oocyst proteins) added, with incubation at 37°C for a further 45 minutes.  
432 The final sample was then washed three times with PBS, dried and Fluoroshield™ with  
433 DAPI (Sigma Aldrich, Cat. No F6057) was added before applying a glass coverslip and  
434 sealing. Slides were visualised by fluorescence microscopy using an Olympus IX82 or  
435 Zeiss Elyra P1 confocal microscope.

436 *Electron microscopy images*

437 Aclar disks of tissue culture were infected and prepared for EM according to the  
438 protocols detailed previously (21).

439 *Ethics Statement*

440 This study was carried out in accordance with Act No 246/1992 Coll. of the Czech  
441 Republic. 419 The protocol was approved by the Committee for Animal Welfare of  
442 Biology Centre Czech 420 Academy of Science and the veterinary administration  
443 authorities with regards to the animal 421 experiments (experiment reference numbers:  
444 114/2013 and 52/2014).

445

446

447 **Abbreviations**

448 NMR: Nuclear Magnetic Resonance

449 DSS: 3-(Trimethylsilyl)-1-propanesulfonic acid, sodium salt

450 PCA: Principal component analysis

451 PLS-DA: Partial Least Squares Discriminant Analysis

452 UV: Ultraviolet

453 HIV: Human Immunodeficiency Virus

454 GC-MS: Gas Chromatography-Mass Spectrometry

455 HDO: Deuterium Oxide

456 IFA: Indirect Fluorescence Assay

457 PCR: Polymerase Chain Reaction

458 DAPI: 4',6-diamidino-2-phenylindole

459 PBS: Phosphate-buffered saline

460 EM: Electron microscopy

461 SCID: Severe Combined Immunodeficiency Disease

462 ATP: adenosine triphosphate

463 AMP: adenosine monophosphate

464 ADP: adenosine diphosphate

465 CoA: Coenzyme A

466 GRIs: glycine reuptake inhibitors

467

468

469 **Declarations**

470 The authors have declared that the research was conducted in the absence of any  
471 commercial or financial relationships that could be construed as a potential conflict of  
472 interest

473 Funding was provided by the BBSRC, Wellcome Trust and a Microbiology Society  
474 Research Visit Grant.

475

476 **Acknowledgements**

477 This research was supported by BBSRC research grant (BB/M009971/1) to Dr.  
478 Anastasios Tsaousis and a Wellcome Trust Equipment Grant 091163/Z/10/Z to Dr.  
479 Mark J. Howard. Christopher N. Miller is supported by a GTA studentship from the  
480 School of Biosciences, University of Kent and a Research Visit Grant award from the  
481 Microbiology Society. Martin Kvac is supported by The Czech Science Foundation  
482 (project No. 15-01090S). We thank Dr. Michelle Rowe for NMR technical support at  
483 Kent and members of the Dr. Tsaousis and Dr. Kvac laboratories for their intellectual  
484 and methodological support. We would also like to thank Matthew Lee and Matthew D.  
485 Badham from the University of Kent for the assistance in using the confocal microscope  
486 and analysing data.

487

488

489

490 **References:**

- 491 1. Kotloff KL, Nataro JP, Blackwelder WC, Nasrin D, Farag TH, Panchalingam S,  
492 Wu Y, Sow SO, Sur D, Breiman RF, Faruque AS, Zaidi AK, Saha D, Alonso PL,  
493 Tamboura B, Sanogo D, Onwuchekwa U, Manna B, Ramamurthy T, Kanungo S,  
494 Ochieng JB, Omore R, Oundo JO, Hossain A, Das SK, Ahmed S, Qureshi S,  
495 Quadri F, Adegbola RA, Antonio M, Hossain MJ, Akinsola A, Mandomando I,  
496 Nhampossa T, Acacio S, Biswas K, O'Reilly CE, Mintz ED, Berkeley LY, Muhsen  
497 K, Sommerfelt H, Robins-Browne RM, Levine MM. 2013. Burden and aetiology of  
498 diarrhoeal disease in infants and young children in developing countries (the  
499 Global Enteric Multicenter Study, GEMS): a prospective, case-control study.  
500 Lancet 382:209-22.
- 501 2. Checkley W, White AC, Jr., Jaganath D, Arrowood MJ, Chalmers RM, Chen XM,  
502 Fayer R, Griffiths JK, Guerrant RL, Hedstrom L, Huston CD, Kotloff KL, Kang G,  
503 Mead JR, Miller M, Petri WA, Jr., Priest JW, Roos DS, Striepen B, Thompson  
504 RC, Ward HD, Van Voorhis WA, Xiao L, Zhu G, Houpt ER. 2014. A review of the  
505 global burden, novel diagnostics, therapeutics, and vaccine targets for  
506 cryptosporidium. Lancet Infect Dis 15:85-94.
- 507 3. Wanyiri JW, Kanyi H, Maina S, Wang DE, Steen A, Ngugi P, Kamau T, Waithera  
508 T, O'Connor R, Gachuhi K, Wamae CN, Mwamburi M, Ward HD. 2014.  
509 Cryptosporidiosis in HIV/AIDS patients in Kenya: clinical features, epidemiology,  
510 molecular characterization and antibody responses. Am J Trop Med Hyg 91:319-  
511 28.

- 512 4. Striepen B. 2013. Parasitic infections: Time to tackle cryptosporidiosis. Nature  
513 503:189-91.
- 514 5. Shirley DA, Moonah SN, Kotloff KL. 2012. Burden of disease from  
515 cryptosporidiosis. Curr Opin Infect Dis 25:555-63.
- 516 6. Caccio SM. 2005. Molecular epidemiology of human cryptosporidiosis.  
517 Parassitologia 47:185-92.
- 518 7. Leoni F, Amar C, Nichols G, Pedraza-Diaz S, McLauchlin J. 2006. Genetic  
519 analysis of *Cryptosporidium* from 2414 humans with diarrhoea in England  
520 between 1985 and 2000. J Med Microbiol 55:703-7.
- 521 8. Wielinga PR, de Vries A, van der Goot TH, Mank T, Mars MH, Kortbeek LM, van  
522 der Giessen JWB. 2008. Molecular epidemiology of *Cryptosporidium* in humans  
523 and cattle in The Netherlands. International Journal for Parasitology 38:809-817.
- 524 9. Widmer G, Sullivan S. 2012. Genomics and population biology of  
525 *Cryptosporidium* species. Parasite Immunol 34:61-71.
- 526 10. Douumbo O, Rossignol JF, Pichard E, Traore HA, Dembele TM, Diakite M, Traore  
527 F, Diallo DA. 1997. Nitazoxanide in the treatment of cryptosporidial diarrhea and  
528 other intestinal parasitic infections associated with acquired immunodeficiency  
529 syndrome in tropical Africa. Am J Trop Med Hyg 56:637-9.
- 530 11. Hussien SM, Abdella OH, Abu-Hashim AH, Aboshiesha GA, Taha MA, El-Shemy  
531 AS, El-Bader MM. 2013. Comparative study between the effect of nitazoxanide  
532 and paromomycine in treatment of cryptosporidiosis in hospitalized children. J  
533 Egypt Soc Parasitol 43:463-70.

- 534 12. Domjahn BT, Hlavsa MC, Anderson B, Schulkin J, Leon J, Jones JL. 2014. A  
535 survey of U.S. obstetrician-gynecologists' clinical and epidemiological knowledge  
536 of cryptosporidiosis in pregnancy. Zoonoses Public Health 61:356-63.
- 537 13. Sparks H, Nair G, Castellanos-Gonzalez A, White AC, Jr. 2015. Treatment of  
538 Cryptosporidium: What We Know, Gaps, and the Way Forward. Curr Trop Med  
539 Rep 2:181-187.
- 540 14. Manjunatha UH, Chao AT, Leong FJ, Diagana TT. 2016. Cryptosporidiosis Drug  
541 Discovery: Opportunities and Challenges. ACS Infect Dis 2:530-7.
- 542 15. Leitch GJ, He Q. 2012. Cryptosporidiosis-an overview. J Biomed Res 25:1-16.
- 543 16. Briggs AD, Boxall NS, Van Santen D, Chalmers RM, McCarthy ND. 2014.  
544 Approaches to the detection of very small, common, and easily missed outbreaks  
545 that together contribute substantially to human *Cryptosporidium* infection.  
546 Epidemiol Infect 142:1869-76.
- 547 17. Karanis P, Aldeybari HM. 2011. Evolution of *Cryptosporidium* in vitro culture. Int J  
548 Parasitol 41:1231-42.
- 549 18. Muller J, Hemphill A. 2013. In vitro culture systems for the study of apicomplexan  
550 parasites in farm animals. Int J Parasitol 43:115-24.
- 551 19. Girouard D, Gallant J, Akiyoshi DE, Nunnari J, Tzipori S. 2006. Failure to  
552 propagate *Cryptosporidium* spp. in cell-free culture. J Parasitol 92:399-400.
- 553 20. Morada M, Lee S, Gunther-Cummins L, Weiss LM, Widmer G, Tzipori S, Yarlett  
554 N. 2016. Continuous culture of *Cryptosporidium parvum* using hollow fiber  
555 technology. Int J Parasitol 46:21-9.

- 556 21. Miller CN, Jossé L, Brown I, Blakeman B, Povey J, Yiangou L, Price M, Cinatl jr  
557 J, Xue W-F, Michaelis M, Tsatsousis AD. 2017. A cell culture platform for  
558 *Cryptosporidium* that enables long-term cultivation and new tools for the  
559 systematic investigation of its biology. Int J Parasitol in press.
- 560 22. Sponseller JK, Griffiths JK, Tzipori S. 2014. The evolution of respiratory  
561 Cryptosporidiosis: evidence for transmission by inhalation. Clin Microbiol Rev  
562 27:575-86.
- 563 23. Wilhelm CL, Yarovinsky F. 2014. Apicomplexan infections in the gut. Parasite  
564 Immunol 36:409-20.
- 565 24. Ng Hublin JSY, Ryan U, Trengove RD, Maker GL. 2012. Development of an  
566 untargeted metabolomics method for the analysis of human faecal samples using  
567 *Cryptosporidium*-infected samples. Molecular and Biochemical Parasitology  
568 185:145-150.
- 569 25. Ng Hublin JS, Ryan U, Trengove R, Maker G. 2013. Metabolomic profiling of  
570 faecal extracts from *Cryptosporidium parvum* infection in experimental mouse  
571 models. PLoS One 8:e77803.
- 572 26. Saric J, Wang Y, Li J, Coen M, Utzinger J, Marchesi JR, Keiser J, Veselkov K,  
573 Lindon JC, Nicholson JK, Holmes E. 2008. Species variation in the fecal  
574 metabolome gives insight into differential gastrointestinal function. J Proteome  
575 Res 7:352-60.
- 576 27. Jacobs DM, Deltimple N, van Velzen E, van Dorsten FA, Bingham M, Vaughan  
577 EE, van Duynhoven J. 2008. (1)H NMR metabolite profiling of feces as a tool to  
578 assess the impact of nutrition on the human microbiome. NMR Biomed 21:615.

- 579 28. Bezabeh T, Somorjai RL, Smith ICP. 2009. MR metabolomics of fecal extracts:  
580 applications in the study of bowel diseases. Magnetic Resonance in Chemistry  
581 47:S54-S61.
- 582 29. Hong YS, Ahn YT, Park JC, Lee JH, Lee H, Huh CS, Kim DH, Ryu DH, Hwang  
583 GS. 2010.  $^1\text{H}$  NMR-based metabonomic assessment of probiotic effects in a  
584 colitis mouse model. Arch Pharmacal Res 33:1091.
- 585 30. Wu J, An Y, Yao J, Wang Y, Tang H. 2010. An optimized sample preparation  
586 method for NMR-based faecal metabonomic analysis. Analyst 135:1023.
- 587 31. Sengupta A, Ghosh S, Das BK, Panda A, Tripathy R, Pied S, Ravindran B,  
588 Pathak S, Sharma S, Sonawat HM. 2016. Host metabolic responses to  
589 Plasmodium falciparum infections evaluated by  $^1\text{H}$  NMR metabolomics. Mol  
590 Biosyst.
- 591 32. Xia J, Sinelnikov IV, Han B, Wishart DS. 2015. MetaboAnalyst 3.0--making  
592 metabolomics more meaningful. Nucleic Acids Res 43:W251-7.
- 593 33. Denis V, Daignan-Fornier B. 1998. Synthesis of glutamine, glycine and 10-formyl  
594 tetrahydrofolate is coregulated with purine biosynthesis in *Saccharomyces*  
595 *cerevisiae*. Molecular and General Genetics MGG 259:246-255.
- 596 34. Marver HS, Tschudy DP, Perlroth MG, Collins A. 1966. Delta-aminolevulinic acid  
597 synthetase. I. Studies in liver homogenates. J Biol Chem 241:2803-9.
- 598 35. Novak P, Tepes P, Fistrice I, Bratos I, Gabelica V. 2006. The application of LC-  
599 NMR and LC-MS for the separation and rapid structure elucidation of an  
600 unknown impurity in 5-aminosalicylic acid. J Pharm Biomed Anal 40:1268.

- 601 36. Abrahamsen MS, Templeton TJ, Enomoto S, Abrahante JE, Zhu G, Lancto CA,  
602 Deng M, Liu C, Widmer G, Tzipori S, Buck GA, Xu P, Bankier AT, Dear PH,  
603 Konfortov BA, Spriggs HF, Iyer L, Anantharaman V, Aravind L, Kapur V. 2004.  
604 Complete genome sequence of the apicomplexan, *Cryptosporidium parvum*.  
605 Science 304:441-5.
- 606 37. Doyle PS, Kanaani J, Wang CC. 1998. Hypoxanthine, guanine, xanthine  
607 phosphoribosyltransferase activity in *Cryptosporidium parvum*. Exp Parasitol  
608 89:9-15.
- 609 38. Clark DP. 1999. New Insights into Human Cryptosporidiosis. Clinical  
610 Microbiology Reviews 12:554-563.
- 611 39. Feng H, Nie W, Sheoran A, Zhang Q, Tzipori S. 2006. Bile acids enhance  
612 invasiveness of *Cryptosporidium* spp. into cultured cells. Infect Immun 74:3342-6.
- 613 40. Gold D, Stein B, Tzipori S. 2001. The utilization of sodium taurocholate in  
614 excystation of *Cryptosporidium parvum* and infection of tissue culture. J Parasitol  
615 87:997-1000.
- 616 41. Kar S, Daugschies A, Cakmak A, Yilmazer N, Dittmar K, Bangoura B. 2011.  
617 *Cryptosporidium parvum* oocyst viability and behaviour of the residual body  
618 during the excystation process. Parasitol Res 109:1719-23.
- 619 42. King BJ, Keegan AR, Phillips R, Fanok S, Monis PT. 2012. Dissection of the  
620 hierarchy and synergism of the bile derived signal on *Cryptosporidium parvum*  
621 excystation and infectivity. Parasitology 139:1533-46.

- 622 43. Kapembwa MS, Bridges C, Joseph AE, Fleming SC, Batman P, Griffin GE. 1990.  
623 Ileal and jejunal absorptive function in patients with AIDS and enterococcidial  
624 infection. *J Infect* 21:43-53.
- 625 44. Goodgame RW, Kimball K, Ou C-N, White AC, Genta RM, Lifschitz CH, Chappell  
626 CL. 1995. Intestinal function and injury in acquired immunodeficiency  
627 syndrome—related cryptosporidiosis. *Gastroenterology* 108:1075-1082.
- 628 45. Augagneur Y, Jaubert L, Schiavoni M, Pachikara N, Garg A, Usmani-Brown S,  
629 Wesolowski D, Zeller S, Ghosal A, Cornillot E, Said HM, Kumar P, Altman S, Ben  
630 Mamoun C. 2013. Identification and functional analysis of the primary  
631 pantothenate transporter, PfPAT, of the human malaria parasite *Plasmodium*  
632 *falciparum*. *J Biol Chem* 288:20558-67.
- 633 46. Tsatsou AD, Kunji ERS, Goldberg AV, Lucocq JM, Hirt RP, Embley TM. 2008. A  
634 novel route for ATP acquisition by the remnant mitochondria of *Encephalitozoon*  
635 *cuniculi*. *Nature* 453:553-556.
- 636 47. Giris M, Depboylu B, Dogru-Abbasoglu S, Erbil Y, Olgac V, Alis H, Aykac-Toker  
637 G, Uysal M. 2008. Effect of taurine on oxidative stress and apoptosis-related  
638 protein expression in trinitrobenzene sulphonic acid-induced colitis. *Clin Exp*  
639 *Immunol* 152:102.
- 640 48. Green TR, Fellman JH, Eicher AL, Pratt KL. 1991. Antioxidant role and  
641 subcellular location of hypotaurine and taurine in human neutrophils. *Biochim*  
642 *Biophys Acta* 1073:91-7.

- 643 49. Zhang M, Izumi I, Kagamimori S, Sokejima S, Yamagami T, Liu Z, Qi B. 2004.  
644       Role of taurine supplementation to prevent exercise-induced oxidative stress in  
645       healthy young men. *Amino Acids* 26:203-7.
- 646 50. Lin S, Sanders DS, Gleeson JT, Osborne C, Messham L, Kurien M. 2016. Long-  
647       term outcomes in patients diagnosed with bile-acid diarrhoea. *Eur J*  
648       *Gastroenterol Hepatol* 28:240-5.
- 649 51. Niggli V, Sigel E, Carafoli E. 1982. Inhibition of the purified and reconstituted  
650       calcium pump of erythrocytes by micro M levels of DIDS and NAP-taurine. *FEBS*  
651       *Lett* 138:164-6.
- 652 52. Yu H, Guo Z, Shen S, Shan W. 2016. Effects of taurine on gut microbiota and  
653       metabolism in mice. *Amino Acids* 48:1601-17.
- 654 53. Seeber F, Soldati-Favre D. 2010. Metabolic pathways in the apicoplast of  
655       apicomplexa. *Int Rev Cell Mol Biol* 281:161-228.
- 656 54. Guo F, Zhang H, Payne HR, Zhu G. 2016. Differential Gene Expression and  
657       Protein Localization of *Cryptosporidium parvum* Fatty Acyl-CoA Synthetase  
658       Isoforms. *J Eukaryot Microbiol* 63:233-46.
- 659 55. Meloni BP, Thompson RC. 1996. Simplified methods for obtaining purified  
660       oocysts from mice and for growing *Cryptosporidium parvum* in vitro. *J Parasitol*  
661       82:757-62.
- 662 56. Milacek P, Vitovec J. 1985. Differential staining of cryptosporidia by aniline-  
663       carbol-methyl violet and tartrazine in smears from feces and scrapings of  
664       intestinal mucosa. *Folia Parasitol (Praha)* 32:50.

- 665 57. Tarrant DJ, Stirpe M, Rowe M, Howard MJ, von der Haar T, Gourlay CW. 2016.  
666 Inappropriate expression of the translation elongation factor 1A disrupts genome  
667 stability and metabolism. *Journal of Cell Science* 129:4455-4465.
- 668 58. Bastow EL, Peswani AR, Tarrant DS, Pentland DR, Chen X, Morgan A,  
669 Staniforth GL, Tullet JM, Rowe ML, Howard MJ, Tuite MF, Gourlay CW. 2016.  
670 New links between SOD1 and metabolic dysfunction from a yeast model of  
671 amyotrophic lateral sclerosis. *J Cell Sci* 129:4118-4129.
- 672 59. Holyoake LV, Hunt S, Sanguinetti G, Cook GM, Howard MJ, Rowe ML, Poole  
673 RK, Shepherd M. 2016. CydDC-mediated reductant export in *Escherichia coli*  
674 controls the transcriptional wiring of energy metabolism and combats nitrosative  
675 stress. *Biochem J* 473:693-701.
- 676 60. Wagstaff JL, Taylor SL, Howard MJ. 2013. Recent developments and  
677 applications of saturation transfer difference nuclear magnetic resonance (STD  
678 NMR) spectroscopy. *Mol Biosyst* 9:571-7.
- 679 61. Anonymous. 2015. Mutlibase for Microsoft Excel, Numerical Dynamics, Japan,  
680 NumericalDynamics.Com.

681

682

683

684

685

686

687 **Supplementary data:**

688 **Supplementary Figure 1: Compound code key**

689 KEGG ID to Compound name conversion table for use with figures 6 and 10.

690

691 **Supplementary Figure 2: Staining of *Cryptosporidium* in faecal samples**

692 Aniline-carbol-methyl violet stain of a faecal smear taken from a mouse in the infection  
693 group. The abundant presence of *Cryptosporidium* (arrows) indicates that the infection  
694 has been successful; and that the animal is producing oocysts. These samples were  
695 acquired at seven days post-infection.

696

697 **Supplementary Video 1: Animation of cellular staining of *Cryptosporidium* using**  
698 **confocal microscopy**

699 3D-stacked animation displaying the localisation of Crypt-a-glo (green), MitoTracker  
700 (red) and DAPI (blue) in a 3D rendering of 31 individual, 0.16 µm thick sections,  
701 overlapping with a final representative thickness of 4.8 µm, displayed in **Figure 1b**.

702

703 **Supplementary Video 2: Animation of cellular staining of *Cryptosporidium* using**  
704 **confocal microscopy**

705 3D-stacked animation displaying the localisation of Crypt-a-glo (green), MitoTracker  
706 (red) and DAPI (blue) in a 3D rendering of 31 individual, 0.16 µm thick sections,  
707 overlapping with a final representative thickness of 4.8 µm, displayed in **Figure 1c**.

708

709 **Supplementary Video 3: Animation of cellular staining of *Cryptosporidium* using**  
710 **confocal microscopy**

711 3D-stacked animation displaying the localisation of Crypt-a-glo (green), MitoTracker  
712 (red) and DAPI (blue) in a 3D rendering of 31 individual, 0.16 µm thick sections,  
713 overlapping with a final representative thickness of 4.8 µm, displayed in **Figure 1d**.

714

715

716

717

718

719

720

721

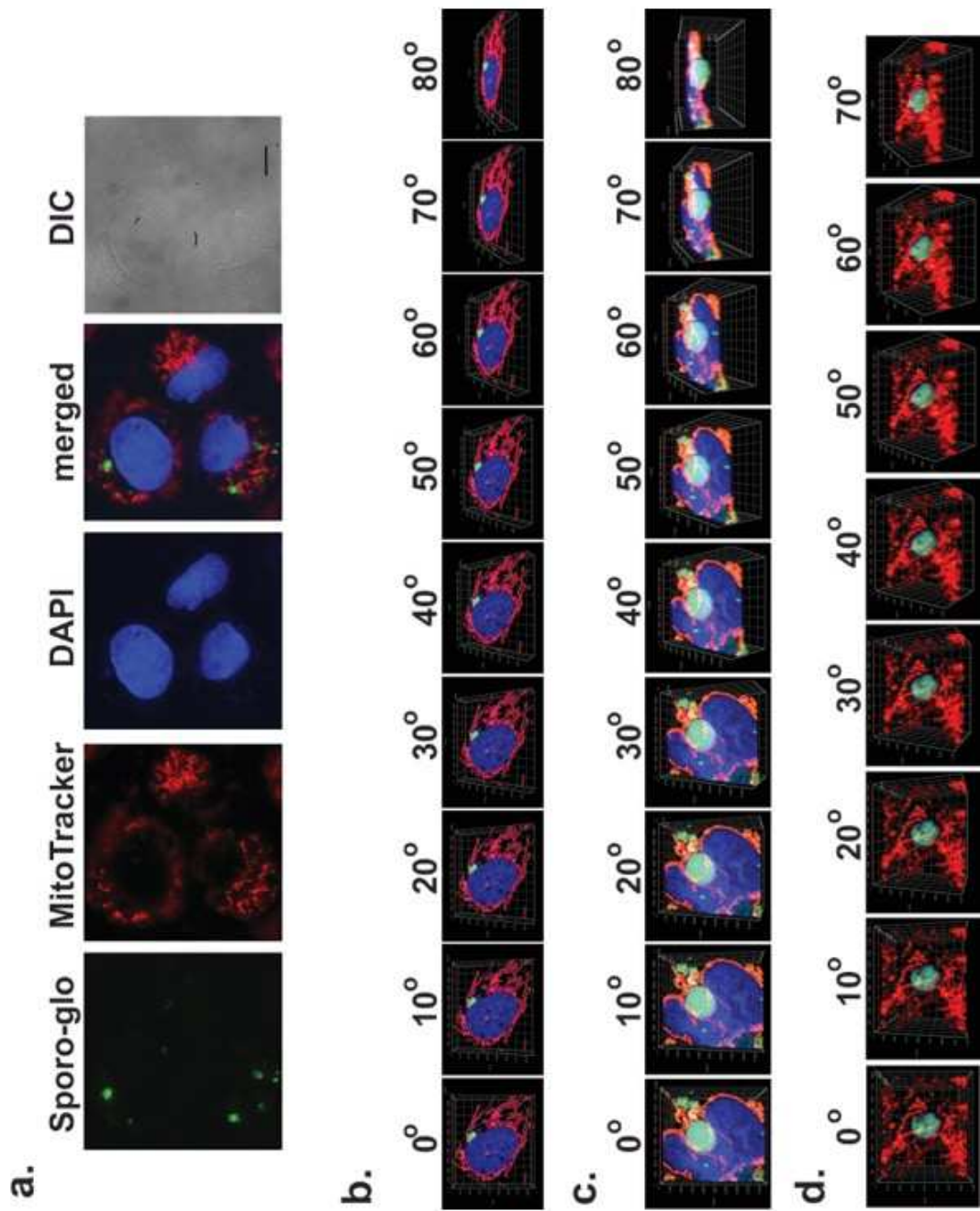
722

723

724 **Figures:**

725

**Figure 1**



726

727 **Figure 1: Indirect Fluorescence Assay of infected cell cultures**

728 **a.** Fluorescence microscopy showing the staining of infected COLO-680N culture with  
729 Sporo-glo (green), MitoTracker CMXRos (red) and DAPI nuclear stain (blue). From the  
730 figure we could observe an obvious mitochondrial “clumping” and polarisation towards  
731 areas of infection, suggesting that the presence of the parasite within a host cell affects  
732 the positioning of host mitochondria or that host mitochondrial concentration somehow  
733 plays a role in determining the site of parasitism. Scale bar: 20  $\mu\text{m}$  **b.** Confocal  
734 microscopy showing the localisation of Crypt-a-glo (green), MitoTracker (red) and DAPI  
735 (blue) in a 3D rendering of 31 individual, 0.16  $\mu\text{m}$  thick sections, overlapping with a final  
736 representative thickness of 4.8  $\mu\text{m}$ . The images are rotated around the x-axis, from 0° to  
737 80°, showing a COLO-680N cell infected with *C. parvum* (green). Individual images of  
738 the stainings were captured in different angles, to show the infection on a three-  
739 dimensional level. A whole video showing a 360° rotation of the three-dimensional z-  
740 stack of the image is found as an animation in **Supplementary Video 1**. **c.** Confocal  
741 microscopy showing the localisation of Crypt-a-glo (green), MitoTracker (red) and DAPI  
742 (blue) in a 3D rendering of 55 individual, 0.16  $\mu\text{m}$  thick sections, overlapping with a final  
743 representative thickness of 8.6  $\mu\text{m}$ . The images are rotated around the x-axis, from 0° to  
744 80°, showing a COLO-680N cell infected with *C. parvum* (green). Individual images of  
745 the stainings were captured in different angles, to show the infection on a three-  
746 dimensional level. A whole video showing a 360° rotation of the three-dimensional z-  
747 stack of the image is found as an animation in **Supplementary Video 2**. **d.** Confocal  
748 microscopy showing the localisation of Crypt-a-glo (green) and MitoTracker (red) in a  
749 3D rendering of 51 individual, 0.16  $\mu\text{m}$  thick sections, overlapping with a final

750 representative thickness of 8.0  $\mu\text{m}$ . The images are rotated around the x-axis, from 0° to  
751 70°, showing mitochondria surrounding an intracellular stage of with *C. parvum* (green).  
752 Individual images of the stainings were captured in different angles, to show the  
753 infection on a three-dimensional level. A whole video showing a 360° rotation of the  
754 three-dimensional z-stack of the image is found as an animation in **Supplementary**  
755 **Video 3.**

756

757

758

759

760

761

762

763

764

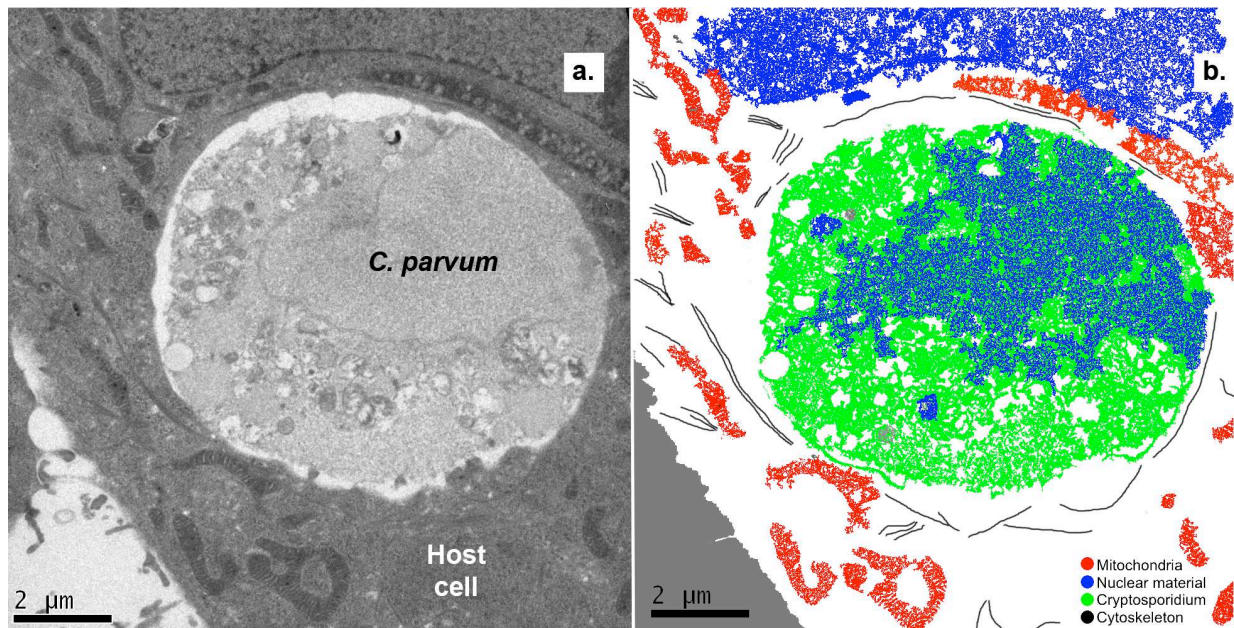
765

766

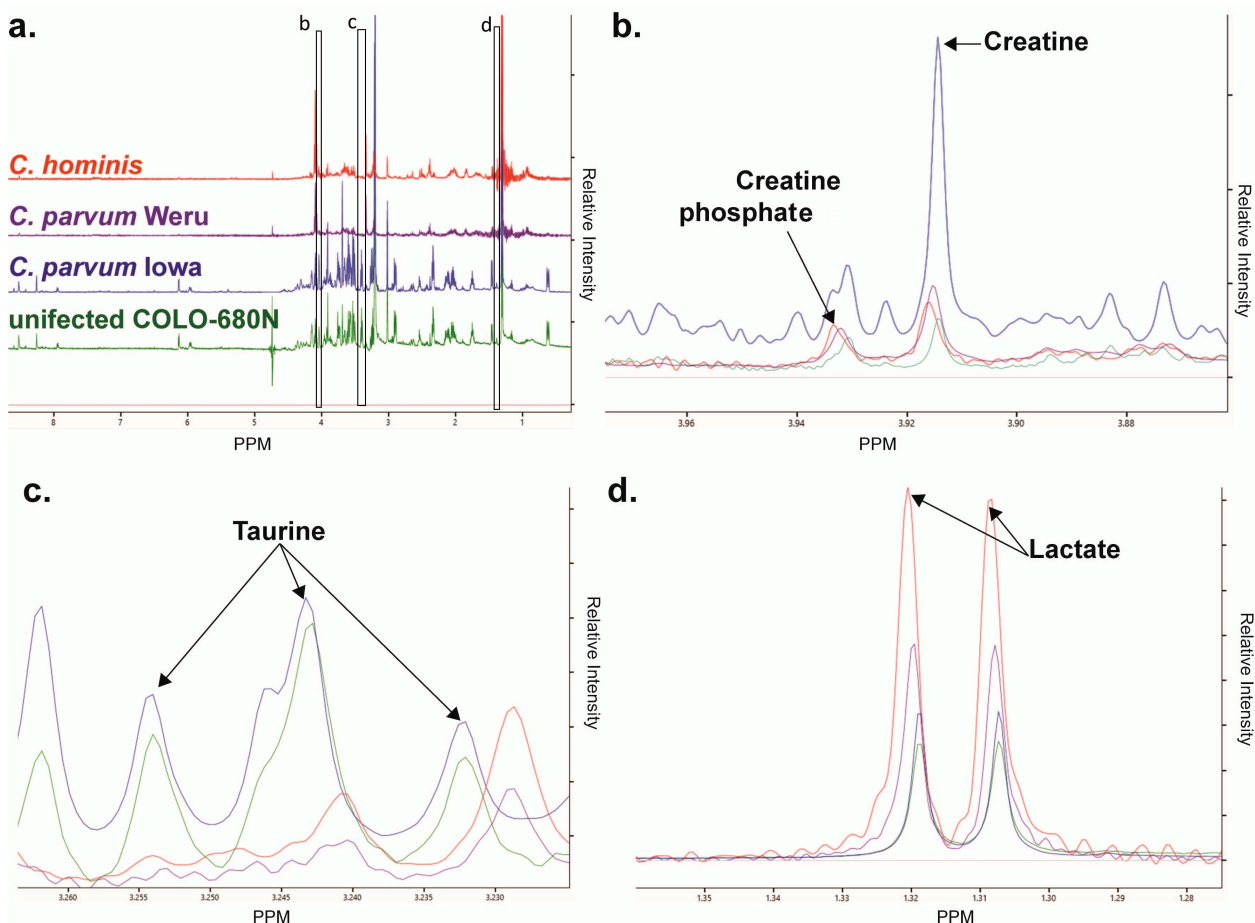
767

768

769

**Figure 2**

782

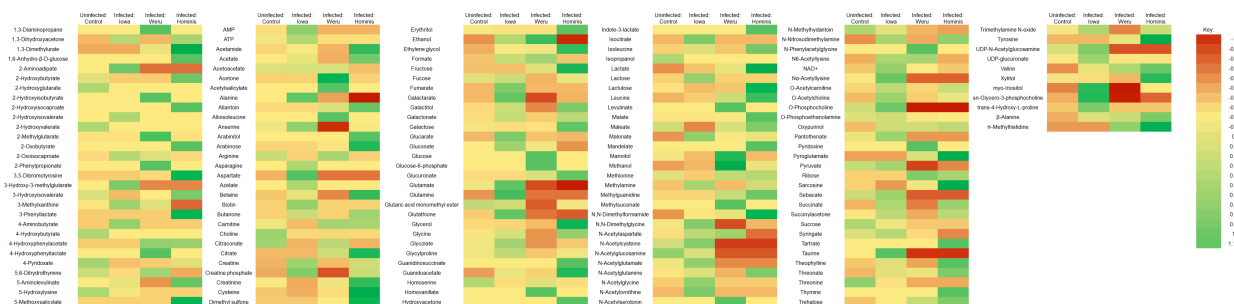
**Figure 3**

783

**Figure 3: Cell Culture infection NMR spectra**

785 **a.** Stacked NMR Spectra produced from the COLO-680N control cultures (green), either  
 786 the *C. parvum* Iowa II (blue), *C. parvum* Weru (purple), or *C. hominis* groups. Direct  
 787 comparisons of the spectra revealed several clearly identifiable differences, including,  
 788 again, differences in creatine and creatine phosphate (**b.**), taurine (**c.**) and lactate (**d.**)  
 789 levels. Noticeably, taurine levels were almost undetectable in *C. hominis* or *C. parvum*  
 790 Weru infections. The spectra displayed are of individual experiments and are  
 791 representative of the spectra observed throughout the groups.

792

**Figure 4**

793

**Figure 4: COLO-680N Experiment Metabolites**

All the metabolites identified by  $^1\text{H}$  NMR analysis in infected and uninfected cells were explored via PCA statistical analysis and the resulting Principal Component values of each individual metabolite recorded. The colour coded heat map represents the significance to which each individual metabolite contributed to the identity of the sample groups. Metabolites that contributed towards variation *within* groupings are coded towards the red, whilst green represents metabolites that stayed relative unvaried within groups but demonstrated variation between groups and thus are of most interest.

803

804

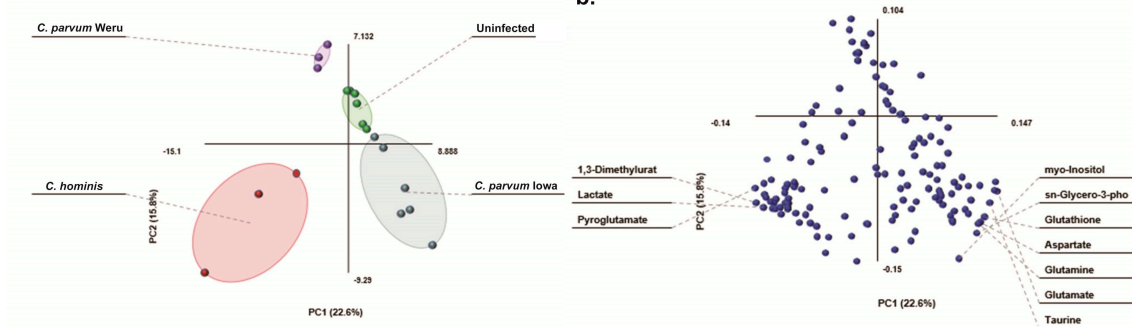
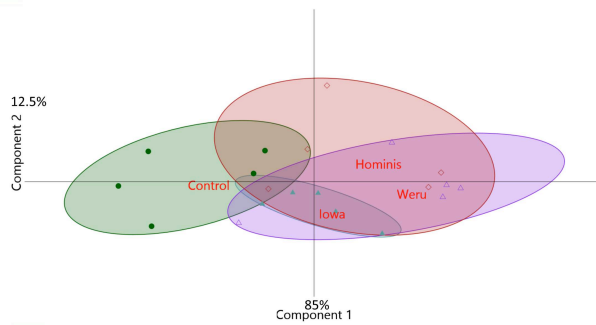
805

806

807

808

809

**Figure 5****b.****c.**

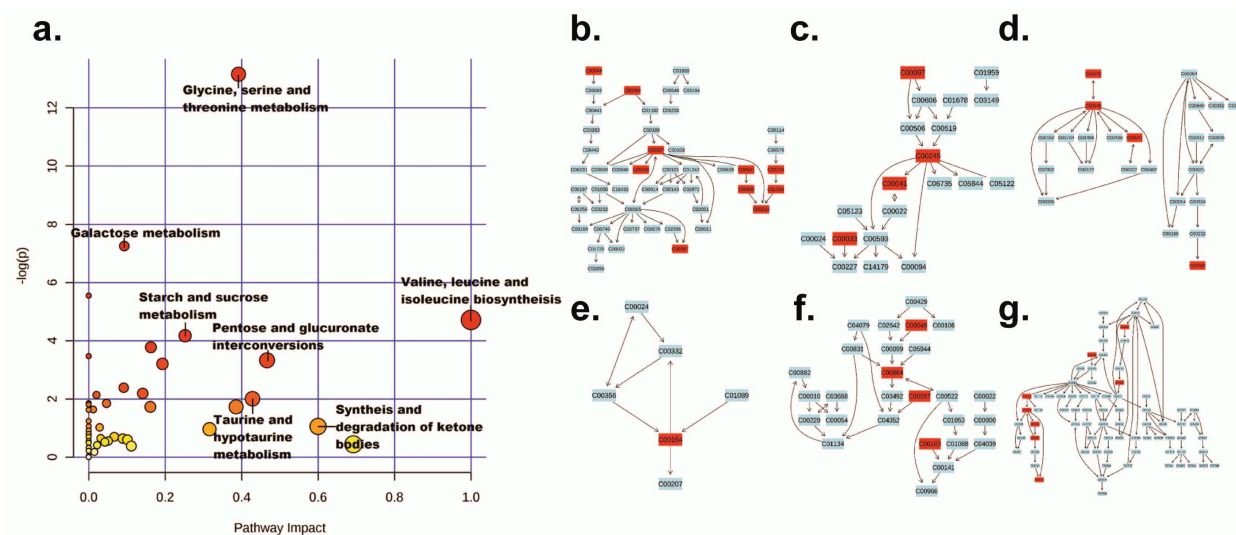
810

**Figure 5: PLS-DA and loading plot of COLO-680N - infected cells NMR results**

811 **a.** PLS-DA statistical analysis of the information provided by the Chenomx screening produced clear groupings, separating the controls (green), *C. parvum* Iowa II infections (blue), *C. parvum* Weru infections (purple) and *C. hominis* infections (red). As the grouping areas do no overlap the separation between the infection conditions again indicates that metabolome differences can be at least in part explained by different *Cryptosporidium* strains/species. **b.** The loading biplot of the PLS-DA analysis shows lactate as a significant contributor to variation, in addition to taurine and myo-inositol among others. **c.** PLS-DA statistical analysis of the information provided by the Chenomx screening using additional samples, also produced clear groupings, separating the controls (green), *C. parvum* Iowa II infections (blue), *C. parvum* Weru infections (purple) and *C. hominis* infections (red).

823

**Figure 6**



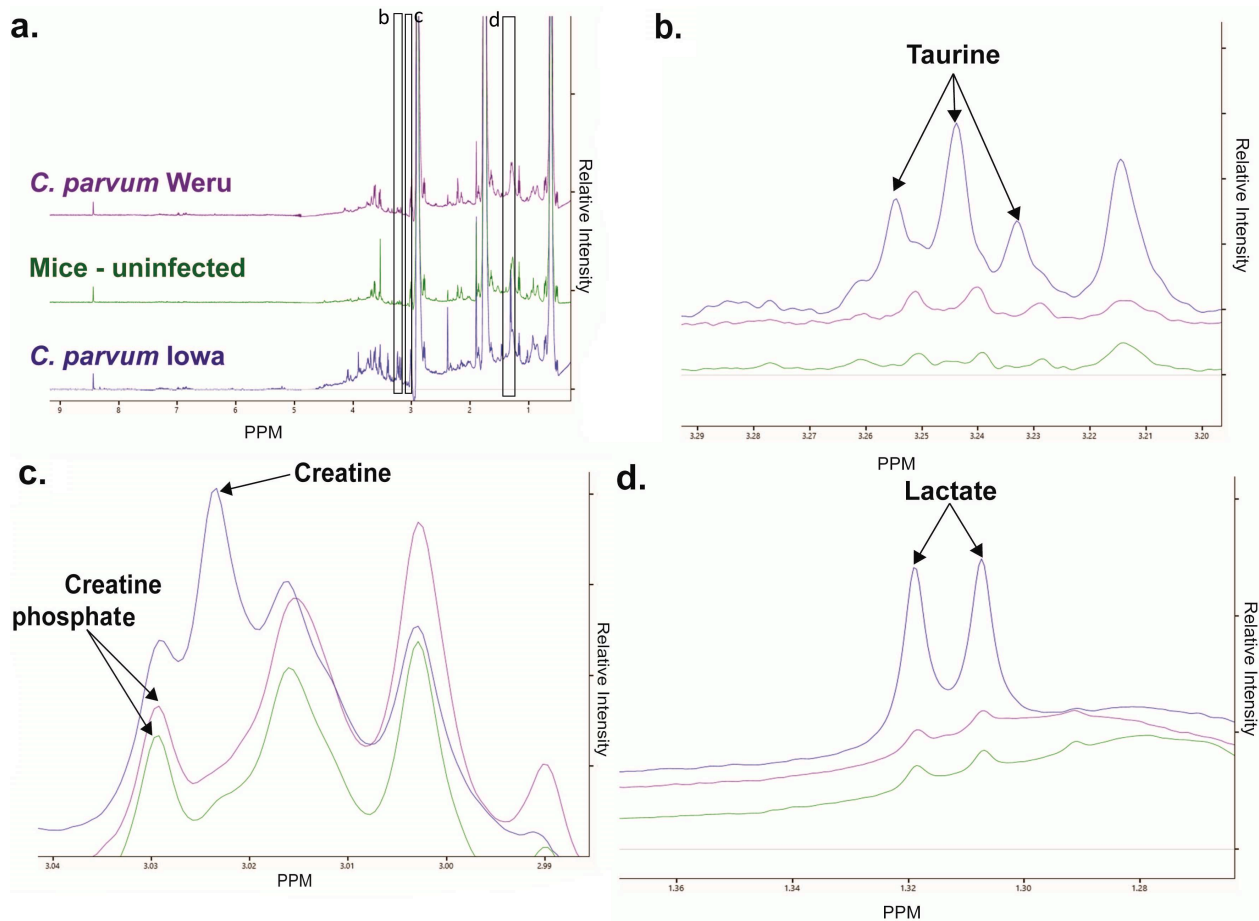
824

825 **Figure 6: Metabolic pathways detected in cell cultures' NMR samples**

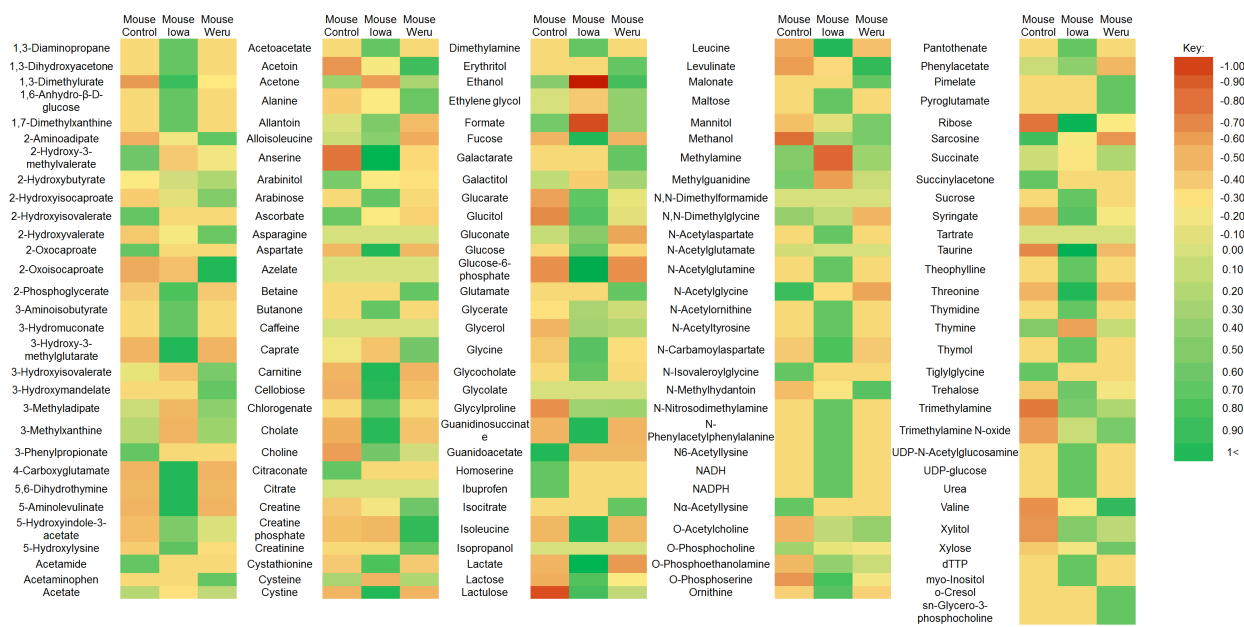
826 a. Data analysed by MetaboAnalyst 3.0, utilising all compounds which displayed some  
827 degree of change as a result of infection, produced a graph of pathways most heavily  
828 impacted (x axis) and pathways containing the most amount of the given compounds  
829 (pathway impact: y-axis), with statistical significance of the predicted pathways  
830 increasing as the colour ranges from yellow (low) to red (high). Six pathways were  
831 chosen to be of particular interest by their position on the graph, with metabolites  
832 present in the experimental samples highlighted in red, including: glycine, serine and  
833 threonine metabolism (b.), taurine and hypotaurine metabolism (c.), Alanine, aspartate  
834 and glutamate metabolism (d.), synthesis and degradation of ketones (e.), pantothenate  
835 and CoA biosynthesis (f.) and arginine and proline metabolism (g.).

836

837

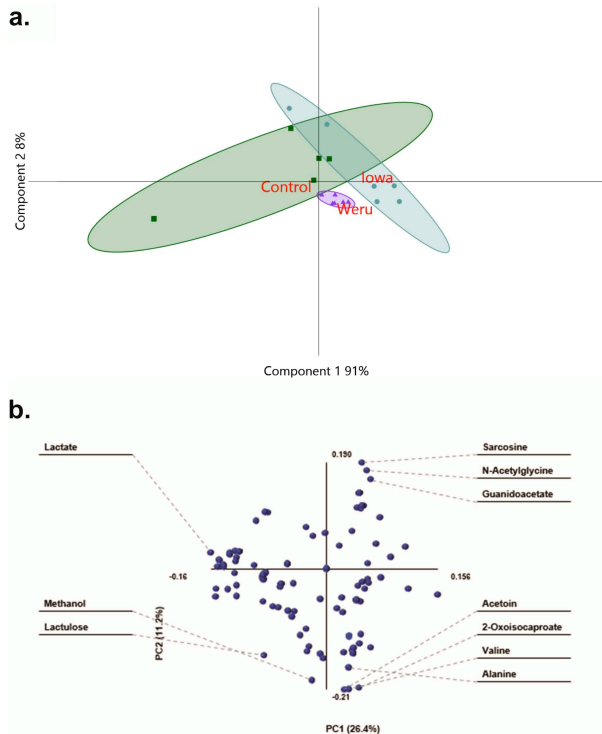
**Figure 7****840 Figure 7: NMR Spectra of mice models of infection**

841 **a.** Stacked NMR Spectra produced from faecal samples of the control mice (green), or  
842 either the Iowa II (blue) or Weru (purple) groups. **b.** Direct comparisons of the spectra  
843 revealed several clearly identifiably differences, including differences in creatine and  
844 creatine phosphate levels. **c.** Levels of taurine were substantially lower in the control or  
845 *C. parvum* Weru samples compared to *C. parvum* Iowa II. **d.** Lactate levels were also  
846 much higher in *C. parvum* Iowa II infected mice compared to the barely detectable  
847 levels in the control mice or *C. parvum* Weru infected groups.

**Figure 8****Figure 8: Mice Experiment Metabolites**

All the metabolites identified by  $^1\text{H}$  NMR analysis in infected and uninfected mice were explored via PCA statistical analysis, the Principal Component values for each metabolite were then recorded. Metabolites that contributed towards variation *within* groupings are coded towards the red, whilst green represents metabolites that stayed relative unvaried within groups but demonstrated variation between groups and thus are of most interest. Yellow represents a general lack of variation between or within groups.

861

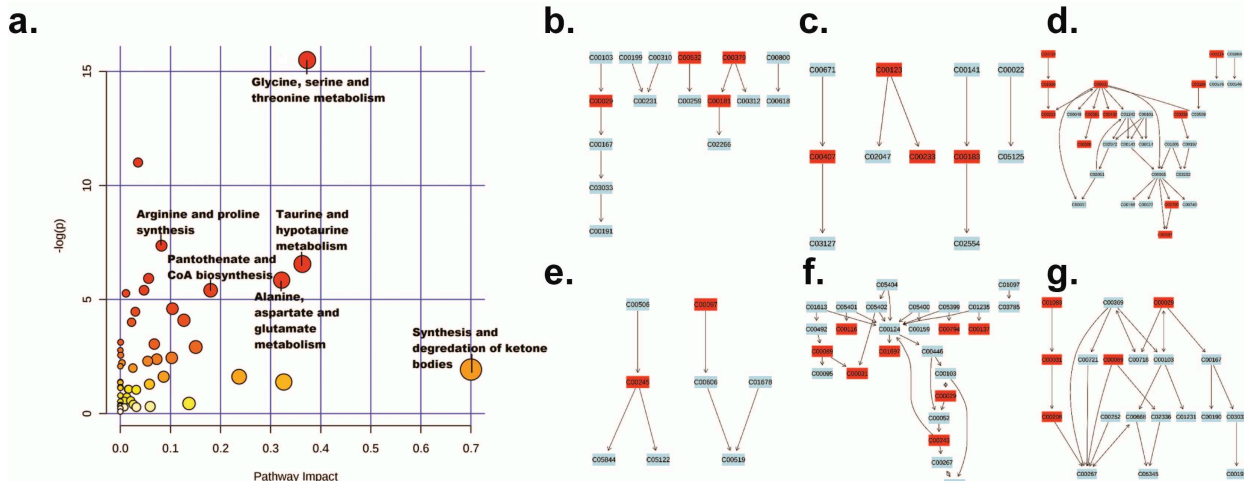
**Figure 9**

862

**Figure 9: PLS-DA and loading plot of mice model NMR results**

863 **a.** PLS-DA statistical analysis of the information provided by the Chenomx screening  
 864 produced clear groupings, separating the controls (green), *C. parvum* Iowa II infections  
 865 (blue) and *C. parvum* Weru infections (purple). As the grouping areas, indicated by the  
 866 areas highlighted, do no overlap, it can be said that the separation between the infection  
 867 conditions represent clear differences in the metabolome, which correspond to the *C.*  
 868 *parvum* strain. **b.** The loading biplot of the PLS-DA analysis shows many of the  
 869 compounds identified by Chenomx contributed towards the separation and groupings.  
 870 Those on the outer most edges, for example alanine, sarcosine, lactate and lactulose,  
 871 had some of the greatest influence on the amount of separation as determined by the  
 872 PLS-DA.

874

**Figure 10**

875

**Figure 10: Metabolic pathways detected in mouse model NMR samples**

**a.** Data analysed by MetaboAnalyst 3.0, utilising all compounds which displayed some degree of change as a result of infection, produced a graph of pathways most heavily impacted (x axis) and pathways containing the most amount of the given compounds (pathway impact: y-axis), with statistical significance of the predicted pathways increasing as the colour ranges from yellow (low) to red (high). Six pathways were chosen to be of particular interest by their position on the graph, with metabolites present in the experimental samples highlighted in red, including: **b.** pentose and glucoronate interconversions, valine, **c.** leucine and isoleucine biosynthesis, **d.** glycine serine and threonine metabolism, **e.** taurine and hypotaurine metabolism, **f.** galactose metabolism and **g.** starch and sucrose metabolism.

887

888

**Figure 11****a**

Shared changes in C. parvum Iowa II infections				
	Mouse	Cells	Pathways	Function
1,3-Dihydroxyacetone			Glycolysis	Energy supply
3-Hydroxy-3-methylglutarate			Ketogenesis	Energy supply
Anserine			Carnosine synthesis	ROS scavenging
Asparagine			Numerous	Numerous
Aspartate			AA Synthesis	
Fucose			N-linked glycosylation	Cell surface signalling
Glycine			Purine synthesis	Numerous
Glycylproline			Collagen synthesis	Connective tissue
Isoleucine			Ketogenesis	Energy supply
N-Acetylaspartate			Numerous	Numerous
N-Acetylornithine			Waste	
N-Nitrosodimethylamine			Carcinogen*	
N6-Acetylysine			Epigenetics	Gene regulation
Pantothenate			Numerous, CoA synthesis	Numerous, Energy Supply
Syringate			Krebs cycle	Energy supply
Taurine			Numerous	ROS, Osmoregulation
UDP-N-Acetylglucosamine			Sugar synthesis	Cytoskeleton and nuclear pore formation
UDP-glucose			Polysaccharide synthesis	Lipid formation
myo-Inositol			Numerous	Cell signalling and mitochondrial quality control

**b**

Shared changes in C. parvum Weru infections				
	Mouse	Cells	Pathways	Function
2-Hydroxybutyrate			Cysteine synthesis	Oxidative stress response
Acetone			Ketosis	Energy supply
citrate			TCA	Energy supply
Creatine			Creatine synthesis	Energy supply
Formate			Folate cycle	Metabolic regulation and methylation
Levulinic acid			Unknown	Potentially Ketosis based energy supply
Mannitol			Mannitol cycle (Non-mammalian)	Potential parasite energy source
Methylguanidine			Protein catabolism	Regulation of inflammation
Pyroglutamate			Glutathione cycle	Glutamate storage
Valine			CoA synthesis	Energy Supply

891 **Figure 11:** Shared changed in metabolite levels between both cell cultures and mice.

892 Those metabolites which showed a reliable contribution towards group separation in

893 both Mouse and cell culture experiments were recorded and their functions assigned.

894 Those metabolites with established direct or indirect involvement with mitochondria

895 were labelled in red. The analysis was conducted for both the Iowa (a) and Weru (b)

896 infection experiments. \*N-Nitrosodimethylamine is a known carcinogen and not naturally

897 produced by any known human or mammalian cell line or any member of the

898 Cryptosporidia and may represent either a contamination or un-characterised spectra

899 peak.